Study of BaTiO$_3$-doped Bi$_2$O$_3$/ZnO varistor microstructure and its electrical characteristics

Faiçal Kharchouche[1], Yousra Malaoui[1], Omrane Bouketir[2]

[1]DAC-hr Laboratory, Department of Electrical Engineering, Faculty of Technology, Setif 1 University-Ferhat ABBAS, Setif, Algeria
[2]Mechatronics Laboratory, Department of Electrical Engineering, Faculty of Technology, Setif 1 University-Ferhat ABBAS, Setif, Algeria

Article Info	ABSTRACT
	This study presents the characterization and optimization of BaTiO$_3$-doped ZnO-based varistors for electrical and electronic applications. The varistors were prepared using a conventional ceramic procedure and were sintered at a temperature of 1,000 °C with different concentrations of BaTiO$_3$ (0 and 3 mol%) added to the Bi$_2$O$_3$/ZnO-based varistor composition (99.5 mol% ZnO and 0.5 mol% Bi$_2$O$_3$). The results showed that the addition of BaTiO$_3$ led to the formation of various oxides and solid solutions, such as Bi$_{12}$TiO$_{20}$, BaTiO$_3$, and (Bi$_2$O$_3$)$_{0.80}$ (BaO)$_{0.20}$. The dielectric constant and grain size decreased with increasing BaTiO$_3$ content, while the non-linearity coefficient, electric fields (Eb) increased, and dielectric loss (Tanδ) decreased. The optimized varistor contains 2 mol% BaTiO$_3$ and an electric field of 148.08 V/mm, which are superior to those of the BaTiO$_3$/Bi$_2$O$_3$/ZnO-based varistor. During this study, we were able to observe that a slight addition of BaTiO$_3$ will increase the breakdown voltage and the coefficient of nonlinearity and this will allow us to develop low-dimensional varistors and install them in the high-voltage domain. *This is an open access article under the CC BY-SA license.*

Corresponding Author:

Faiçal Kharchouche
DAC-hr Laboratory, Department of Electrical Engineering, Faculty of Technology
Setif 1 University-Ferhat ABBAS
Setif, Algeria
Email: faical.kharchouche@univ-setif.dz

1. INTRODUCTION

Varistors made of Zinc oxide (ZnO) are polycrystalline ceramic semiconductors, non-linear resistors that are used for protecting electronic components and electrical installation from surges. They are also largely employed to stabilize voltage and suppress transient surges in electric power systems as well as in electronic circuits. Various types of such varistors are being used in lightning arrestors [1]–[6]. The chemical constitution of this type of varistors; is 98% mol of ZnO and 2% represents additives. The non-linearity of I-V characteristics is due to the formation of double Schottky barrier layers at the grain boundaries. Commercial ZnO-Bi$_2$O$_3$ varistors are traditionally manufactured by mixing the oxides in a direct manner, where it is not easy to get the exact desired microstructure and hence the electrical proprieties [7]–[12]. The choice of a good chemical structure and composition will determine the non-linear coefficients of the varistors. These coefficients are determined through extensive experimental and empirical studies. Adding metal oxides during manufacturing or shaping will alter the electrical properties and/or the microstructure of the final product [13]–[15]. In the subsequent sections, the main constituents of a varistor are introduced. The effects of these elements on material properties are also investigated. Special emphasis will be on the conditions of further development of ZnO-based varistors to achieve optimal manufacturing processes.

Production of varistors by the longest method of sintering a mixture of ZnO powder as a milieu and small amounts of metal oxides such as $SrTiO_3$, SnO_2, WO_3, Bi_2O_3, TiO_2, Sb_2O_3, CeO_2 is discussed in [14]–[21].

These oxides have been considered because of their wide bandgap properties (Eg> 3 eV). Some studies have also been conducted to investigate the influence of specific dopants such as Ce_2O_3, Ho_2O_3, La_2O_3, Dy_2O_3, and Y_2O_3 [22]–[24]. The following relationship was used to determine the variation of current I as a function of voltage V and determine the coefficients of non-linearity for varistors [25]–[27].

$$I = kV^{\alpha} \tag{1}$$

or

$$J = kE^{\alpha} \tag{2}$$

α signifies the coefficients of non-linearity, E is the electric field and J is the electric current density. This study focuses on the effects of the $BaTiO_3$ perovskite type as an addition to a matrix consisting of 99.5% ZnO + 0.5% Bi_2O_3 and microstructure analysis and electrical properties were studied on all samples.

2. EXPERIMENTAL PROCEDURE

Powder of Nano ZnO with high purity (99.99% Nanogard) and particle size of 60 nm was considered in this study. Bi_2O_3 powder was added to the ZnO with standard proportion according to the formula below: 99.5% ZnO + 0.5% Bi_2O_3 (all in mol%). Four samples Z0 (ZB), Z1 (ZB+1mol% $BaTiO_3$), Z2 (ZB+2mol% $BaTiO_3$), and Z3 (ZB+3mol% $BaTiO_3$) were prepared for the experimental investigation. The basic composition of this formula is: 99.5% ZnO + 0.5% Bi_2O_3 + X mol% $BaTiO_3$ (ZB + X mol% $BaTiO_3$). Our experimental protocol for the elaboration of varistors was carried out using the classic method of mixing oxides. A small amount (approximately 50 g) of the selected powder is mixed in a polypropylene bottle filled with 5 mm diameter zirconia beads in deionized water containing the zirconia beads and ethanol using a mixer. The mixing operation took 3 hours with a rotation speed (2 rpm) using zirconia beads, these beads promote the homogenization of the mixture and prevent pollution of the mixture. The powder is dried at 110 °C for 12 hours. Then calcined isothermally at 800 °C for 2 hours (rise rate 10 °C/min). However, the powder mixture was ground and after this step, it was sieved through a 200 µm sieve. before pressing and for each sample, we use 0.5 g of powder and 4% polyvinyl alcohol (PVA) as an organic binder. This results in the formation of so-called "soft" deformable agglomerates that support particle alignment during pressing. Incorporate in a porcelain mortar at the rate of 2 drops per 10 g of powder to form a paste. during this operation several advantages can be found among which the relative density will increase, that is to say, the porosity will decrease which can be seen through the scanning electron microscopy SEM on the microstructure of each sample also the use of PVA will be prevented the creation and appearance of cracks which will disrupt and degrade the electrical characteristics. After drying the latter in an oven at 80 °C for 1h, it is extracted, ground in a mortar, and passed through a 200 μm sieve. Our technique consists of shaping starting powder. We implemented two complementary compression protocols. A uniaxial pressure of 40 MPa was applied to the powder mixture in a cylindrical press to obtain the desired shape. Then an isostatic pressure of 300 MPa was applied for 5 minutes on all samples. The final dimensions of the samples after pressing are approximately 8 mm in diameter and approximately 1.5 mm in thickness. Sintering all samples at 1,000 °C at a speed of 5 °C/min for 2 hours, sintering considers the last stage of the development of the sample as illustrated in Figure 1 which presents the different stages of the development of the varistor. Using the Archimedes method, we were able to measure and determine the density of the sample. High-resolution SEM was used to understand the microstructural changes and monitor the microstructural evolution, and the mapping of the four samples was also examined by EDX (Hitachi S-3500N). Using the linear intercept method to calculate the grain size [4]–[7], [19]. Using this method, several segments of length L were traced on the micrograph, and the number N of intercepted grains was counted. Grains not completely cut are counted as half a grain, as presented by Mendelson [17], [18], the average grain size G is determined by this expression.

$$G = 1.5 \cdot L/MN \tag{3}$$

Where M is the magnification of the micrograph, L is the random line length on the micrograph, and N is the number of grain boundaries intercepted by the lines. A thin layer of silver paste is applied to both sides of the pellet and annealed in a conventional oven at 650 °C for 10 min to establish better contact with the electrode whose diameter was 10 mm. The parameters E_b is the breakdown field, J_L is the leakage current, and α could

then be determined from the use of a voltage source with an integrated nanometer (measure source unit, Keithley 237) which determines the current/voltage characteristics. By convention, we define the non-linearity coefficient α as,

$$\alpha = \frac{(log J_2 - log J_1)}{(log E_2 - log E_1)} \tag{4}$$

with $J_1 = 1$ mA.cm^{-2} and $J_2 = 10$ mA.cm^{-2}. Graphically, it corresponds to the slope of the log J = f (log E) curve. As part of this work, we were interested in some of these parameters, in particular, the dielectric constant ε', the loss factor ε", and the loss tangent tanδ. These parameters were measured using an impedance analyzer HP4194A. Also, the dielectric constant could be calculated using (5). The relative permittivity ε_r is given by:

$$\varepsilon r = C/Cv \tag{5}$$

where C is the capacity of the material under test and Cv is the capacity of air. In an alternating electric field, the complex dielectric permittivity ε given by:

$$\varepsilon = \varepsilon'(\omega) - j\varepsilon''(\omega) \tag{6}$$

where ε' is the dielectric constant, ε" is the dielectric loss factor (the dielectric dissipation factor). It is given by (7):

$$tan\delta = \varepsilon''/\varepsilon' \tag{7}$$

a horizontal pushrod dilatometer Dil 402 PC (Netzsch) with a temperature range of 25–1,400 °C was used for dilation measurement. Pellets with a diameter of 7 mm were pressed at a pressure of 1t for 20 s. Then they were sintered at a constant heating rate of 5 °C/min and held at 1,000 °C for 2h before they were cooled to room temperature in air.
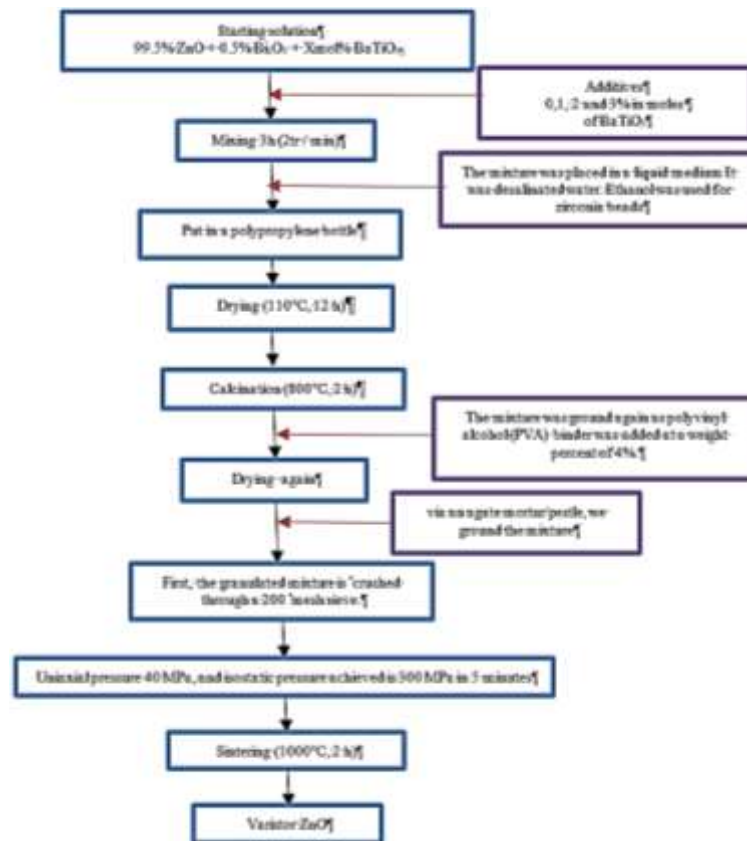

Figure 1. Diagram, presenting the different stages of varistor elaboration

3.   RESULTS AND DISCUSSION

We have chosen to work on three commercial powders. They have heterogeneous grain sizes, according to the SEM image of Figure 2. It can be seen that the agglomeration of the commercial ZnO powder is composed of grains of the lower order of 1 μm, and a very weak agglomeration. Regarding the commercial powder of barium oxide titanate (BaTiO$_3$), we see that the grains are very fine in the order of a nanometer.

3.1. Microstructural studies
3.1.1. EDX mapping

The study of the micrograph and the analysis of the SEM images according to the experimental protocol of sintering varistors at a temperature of 1,000 °C for 2 hours makes it possible to precisely illustrate the sizes of precipitates and shows secondary phase precipitation on a fractured surface of the sample Z1 as shown in Figure 3. The result of this study is supported by EDX mapping which allowed us firstly to see all the chemical components incorporated into the main zinc oxide matrix of the varistor and also shows that these secondary phases are rich in Ti and Ba but completely free of ZnO and bismuth. The microstructure is quite homogeneous (no bimodal distribution). The cracking is intergranular. We have only seen extra-granular porosities since the intra-granular porosities are specifically spherical and localized in the grains. We are therefore dealing with normal growth of the microstructure without pore-grain boundary separation and then abnormal growth.

Small porosities are observed at the grain boundaries and on the faces of the grains as well as a liquid phase (white) at the triple points and at the grain boundaries. White nodules are observed in the middle of the faces of the grains and perhaps inside the grains. It is difficult to tell if the white nodules are inside the grains since the fracture is essentially intergranular.

The liquid phase is observed at the grain boundaries but not between the grains. On the other hand, the white nodules are located on the faces of the grains and sometimes at the triple points. The hypothesis that can be made is that the nodules have a different composition from the liquid phase.

Figure 4 Let's take a look at the SEM-EDX elemental mapping for one of the samples which contain all the stoichiometry required in this study: (99.5% ZnO + 0.5% Bi$_2$O$_3$ + 1% BaTiO$_3$) (all in mol%). The electron image shows the distribution of chemical elements in the internal matrix of the samples, this image shows two very important points such as the homogeneous dispersion of atoms and the appearance of secondary phases through the chemical reactions after sintering, the corresponding elementary element maps are (Zn, Ba, Bi, Ti, and O). The spectrum of the EDX region and the table of atomic and weight ratios of the different elements obtained after the sintering process. Grain boundary analysis by EDX indicates that the grain boundary between grains is richer in Ba, Ti, and Bi and sometimes at triple points compared to other elements (Zn, Ba, Bi, Ti, and O), so there is the possibility of a chemical reaction at the grain boundary.

3.1.2. Dilatometry

Dilatometry is the measurement of change in a linear dimension of a sample during a programmed thermal cycle. In principle, therefore access to the change in volume of a sample subjected to a thermal program, through an appropriate combination of measures linear. The dilatometer measures the linear variation in the dimension of a sample up to a temperature of 1,400 °C in this work and under a controlled atmosphere. This device is very useful for following shrinkage during sintering according to the time and temperature and provides access to the expansion coefficients of sintered materials. Figure 5 illustrates the full cycle of the sintering shrinkage process. The main events in this process are shown; these include mainly the temperature of the sintering beginning, the temperature of the start point of densification (950 °C), and the point where the open porosity is eliminated. Moreover, the final phase of sintering where the gradient is big with a final linear shrinkage of the neighborhood (0.08) is demonstrated as well. The shrinkage behavior during sintering in our case of varistor production is due to the existence of the liquid phase of the varistor substance, which contains additives like Bi$_2$O$_3$ and BaTiO$_3$.

3.1.3. SEM observation

Figure 6 shows the microstructure of the varistors observed by scanning electron microscope on the fractures after metallization with gold. The micrographs of the varistors show that the varistors are quite dense. These justify the high densities obtained. They also show distinct grain boundaries, very low intergranular porosity, and homogeneous grain distribution in each sample. The average grain sizes are shown in Table 1. Table 1 presents the approximate values of the grain size which varies respectively from 3.12 μm to 2.5 μm for Z0 to Z3. It is shown from the microstructure analysis that there were no significant differences in the shape of the grains of the four samples. However, there are substantial differences in their grains' size, where it is notably small for Z3 as compared to other samples. It should be noted that the more quantity of BaTiO$_3$ powder we add to the sample, the more we notice that there is a reduction in grain size.

It is also mentioned that the appearance of the precipitation of secondary phases and nodal points at grain boundaries will lead to the augmentation of grain size. These microstructures present a significant proportion of sub-joints and are characterized by a bimodal distribution of grain sizes. In addition, the microstructure shows the composition of a massive phase and an intergranular phase. The sample Z0 appears to be further porous compared to the other three samples which are doped by $BaTiO_3$, the amount of $BaTiO_3$ added improves grain size and advances micro-structural uniformity. All of these results are in agreement with the work cited in references [17]–[22]. The measured density values are given in Table 1, the density varies respectively from 93.42, 95.42, 96.06, and 96.86 for Z0, Z1, Z2 to Z3. So, we notice that the density of the samples improves as we add a quantity of $BaTiO_3$ powder. In this case, we can say that the porosity has decreased due to the powder effect of $BaTiO_3$.
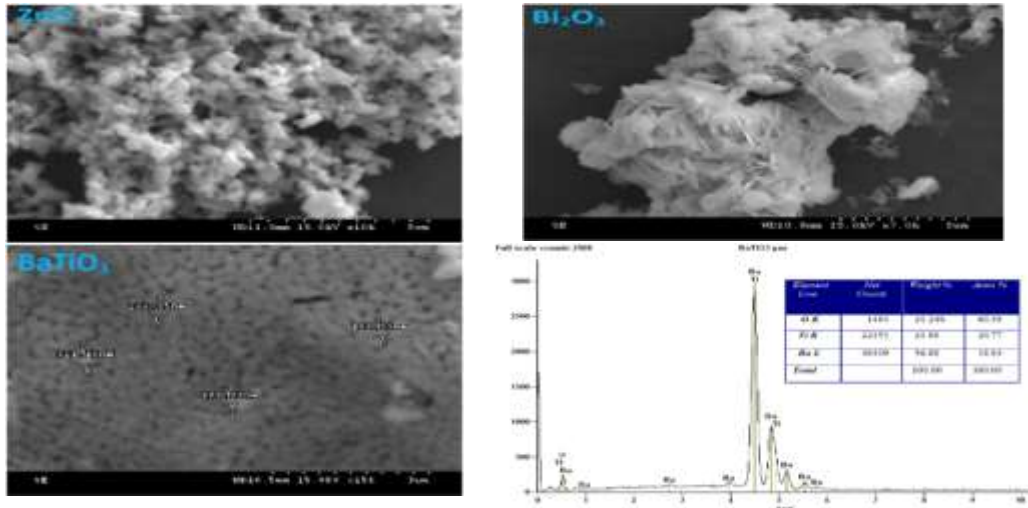
Figure 2. SEM image of Bi_2O_3, $BaTiO_3$, and ZnO powder
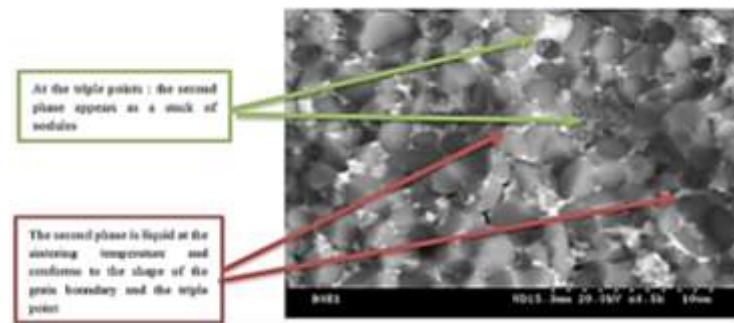
Figure 3. Presentation of the micrograph of a fractured surface by SEM for sample Z1

3.1.4. XRD analysis

Figures 7 and 8 show a typical X-ray diffractogram (XRD) of a zinc oxide varistor from sample Z1 and all samples, recorded on all the samples at 1,000 °C for 2 h, calcined at 800 °C. According to the JCPDS data sheet (01-089-7102) presented in Figures 7 and 8, the lines constituting these spectra are the well characterization of ZnO crystallizing in the hexagonal structure and which is featured by a peak looking at an angle of $2\theta = 36.256°$. In these spectra, we observe the presence of small lines corresponding to the secondary phases of the doping elements, we obtained three phases with weak peaks like $Bi_{12}TiO_{20}$ has a compound name ($GD*-\backslash Bi_2O_3\backslash$), $BaTiO_3$, and $(Bi_2O_3)_{0.80}(BaO)_{0.20}$, has a compound name (Bismuth Barium Oxide) according to the JCPDS data sheet (00-042-0186), (01-074-1968) and (00-032-0109) which indicates that there is a dissolution of the Bi_2O_3 and $BaTiO_3$ dopants within the ZnO crystal lattice by occupying the Zn ionic sites. Note also that the spectra show that, for all the pure and doped samples, the line diffracted by the (101) planes are the most intense. It is deduced that the solid solutions that are detected by XRD are situated in the grain limitations of ZnO. As shown in the SEM of Z1 (Figure 2).
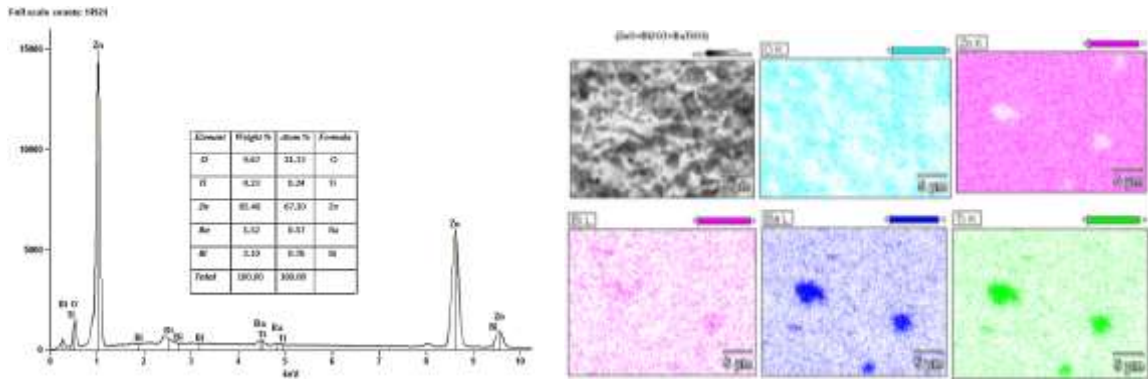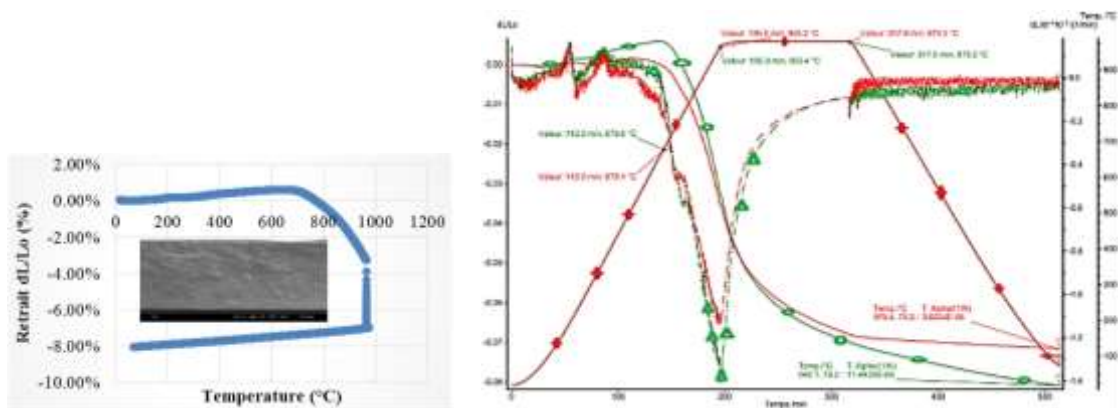
Figure 4. EDX mapping of sample Z1

Figure 5. Dilatometric shrinkage curves of varistor Z1

3.2. Electrical properties

The electrical characteristics E=f(J) of the studied samples is given in Figure 9. These samples have been sintered at 1,000 °C for 2 hours as stated above. It is clear from the curves that all samples have the same E=f(J) shape. However, the values of the current densities and electric fields are very different from one sample to another. The addition of the doping powder $BaTiO_3$ increased the nonlinear coefficient and the electric field in the Bi_2O_3-based ZnO varistor. The nonlinearity coefficients measured for each varistor are shown in Table 2. The existence of the nonlinearity region is the most important property of varistors. The varistors present their conducting phase here. The current increases much faster than the voltage in this region of nonlinearity. So, the electrical characteristics obtained through this elaboration of Bi_2O_3-based ZnO varistor doped with $BaTiO_3$ illustrate the transition from the insulating phase to the conductive phase, has occurred very fast.
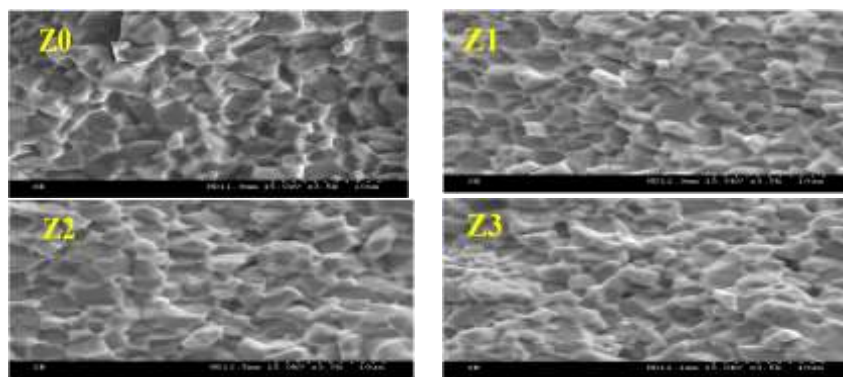

Figure 6. Presentation by MEB of all samples with/without $BaTiO_3$ sintered at 1,000 °C

Table 1. The main data of the microstructural

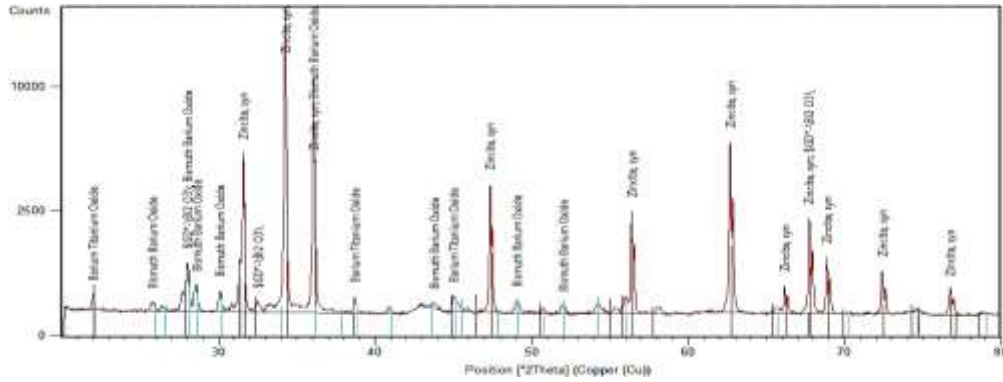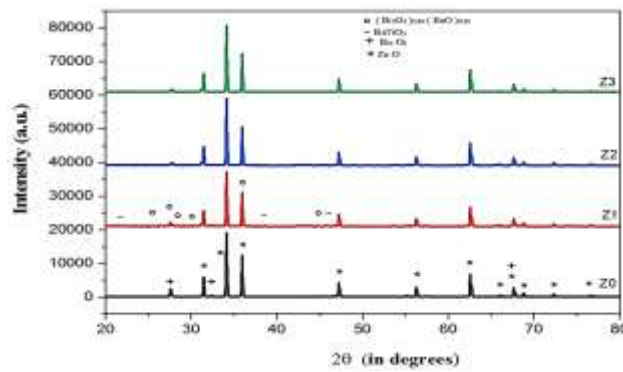| Composition (99.5% ZnO + 0.5% Bi_2O_3)+Xmol% $BaTiO_3$)	Grain size (µm)	Relative density (%)
Z0 (x=0)	3.12	93.42
Z1 (x=1)	2.88	95.42
Z2 (x=2)	2.67	96.02
Z3 (x=3)	2.5	96.86

Figure 7. X-ray diffractogram (XRD) of a zinc oxide varistor from sample Z1

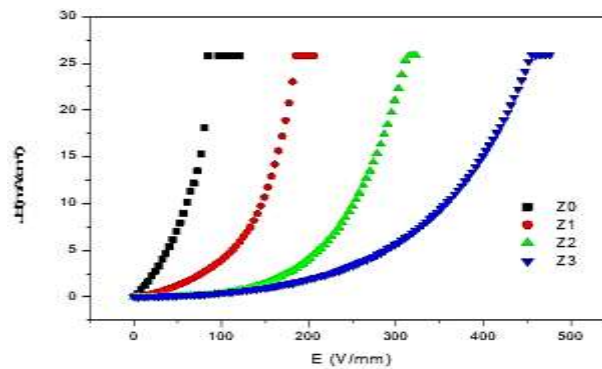Figure 8. X-ray diffractogram (XRD) of all samples sintered at 1,000 °C

Figure 9. J-E characteristic of all samples sintered at 1,000 °C

Table 2. The main data of the electrical characterization

Composition (99.5% ZnO + 0.5% Bi_2O_3+Xmol% $BaTiO_3$)	Breakdown field Eb_{1mA} (V/mm)	The nonlinearity coefficients α
Z0 (x=0)	12.09	1.53
Z1 (x=1)	44.35	2.03
Z2 (x=2)	148.08	3.58
Z3 (x=3)	176.15	2.74

3.3. Dielectric property

The evolution of the real part ε' and the imaginary part ε'' of the permittivity as a function of frequency are first carried out at room temperature on all samples with and without BaTiO₃. Figure 10 regroups the permittivities of the four samples in the interval of 100-2 MHz. ε' decreases quickly at the beginning and then stabilizes when the frequency increases. On the other hand, the loss tangents ε'' present very low values, not exceeding 0.1. We can deduce that ε' decreased with the increase in the concentration of BaTiO₃. From these results, we see that the surfaces and grain boundaries of the samples can be charged and contain charge carriers which can orient themselves under the action of an electric field and thus contribute to the polarization of the material. This phenomenon is called the interfacial polarization mechanism. It is inferred that there is a decrease in the number of conductive carriers, which may accompany the test frequency during the dielectric constant. It should be noted that the dissipation factor at 10 kHz shows a fluctuation between 0.119 and 0.32 as the amount of BaTiO₃ increases. The tanδ of the dielectric property includes heat loss in joules due to leakage current and heat loss due to friction due to rotation of the electric dipole [24]. It is believed that the reason all samples have high tanδ is that the leakage current is quite high. More detailed dielectric property parameters are summarized in Table 3.

The dielectric constant is an important parameter in the design of passive devices for integrated circuits and advanced packaging technologies. Figure 11 demonstrates that the dielectric constant is inversely proportional with the frequency in the range of 1 kHz to 2 MHz after heating at different temperatures. For most dielectric materials, the dipole rotation rate at high frequencies is insufficient to accommodate changes in applied AC bias voltage, so dielectric relaxation is expected to decrease the permittivity with increasing frequency. We also found that the decrease in permittivity with increasing temperature is uniform at low and high frequencies.
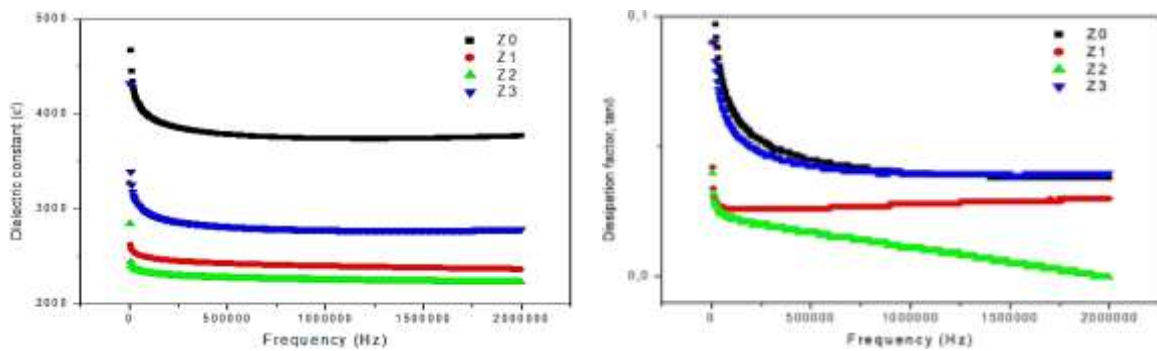

Figure 10. Evolution of dielectric constant and dielectric loss versus frequency
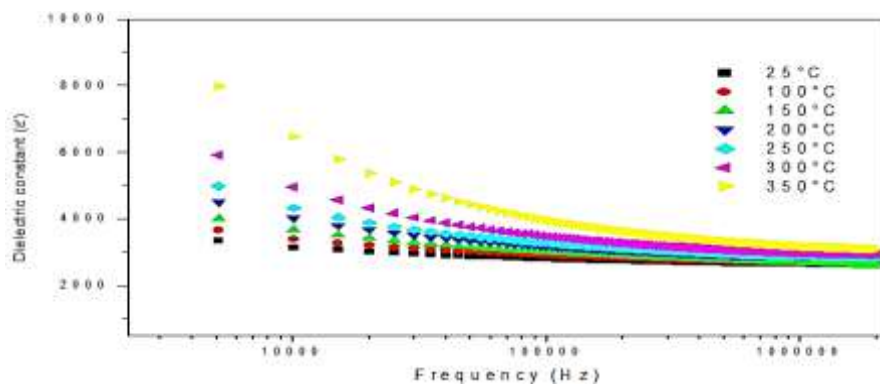

Figure 11. Evolution of dielectric constant versus frequency for sample Z1

Table 3. The main data of the dielectric characterization

Composition (99.5% ZnO + 0.5% Bi₂O₃)+Xmol% BaTiO₃)	Dielectric constant ε'(10KHz)	Dielectric loss Tanδ (10KHz)
Z0 (x=0)	4444	0.119
Z1 (x=1)	2576	0.034
Z2 (x=2)	2404	0.032
Z3 (x=3)	3246	0.102

4. CONCLUSION

This study consists of three main parts. Thus, we focus in the first part on the development and elaboration process of the varistors, while the second part depends on the precise microstructural characterization, and the third on the electrical and dielectric properties. $BaTiO_3$-doped Bi_2O_3/ZnO varistors were developed traditionally. The added amount of $BaTiO_3$ is 0 to 3 mol%. The sintering temperature chosen in this work is 1,000 °C. The results are summarized below; i) Expansion measurements show that the samples started to shrink at the wanted temperature, with compression onset at 950 °C; ii) As the $BaTiO_3$ concentration increases, the grain size of the sample significantly reduces from 2.16 µm to 1.89 µm; iii) XRD analysis confirmed the formulation of the ZnO hexagonal crystal structure. According to the JCPDS database (01-089-7102), all major peaks can be indexed as zinc oxide phases. The spectrum of Z1 shows that the microstructure consists of three phases: ZnO grains (primary phase) and other solid phases, $Bi_{12}TiO_{20}$, $BaTiO_3$, and $(Bi_2O_3)_{0.80}$ $(BaO)_{0.20}$, described by the appearance of peaks; iv) Determine the nonlinear coefficients of the curve E=f(J). This study shows that as the BaTiO3 content increases, the nonlinear coefficients increase; v) The electric field (Eb) and relative density as the grain size increases; vi) When we use a small amount of $BaTiO_3$, the dielectric constant and dielectric loss will decrease; vii) The findings suggest that $BaTiO_3$-doped ZnO-based varistors have the potential for use in electrical and electronic applications requiring high-performance non-linear behavior.

REFERENCES

[1] F. Kharchouche and A. Zebar, "Influence of SrCO3-doping on the microstructure and electrical properties of ZnO–(Bi2O3/Sb2O3) varistor ceramics," *Journal of Materials Science: Materials in Electronics*, vol. 34, no. 9, p. 776, Mar. 2023, doi: 10.1007/s10854-023-10092-8.

[2] L. Muremi and P. N. Bokoro, "Ageing characterisation of varistor arresters: a statistical model for grain response under applied thermal stress," *Journal of Electrical Engineering and Technology*, vol. 16, no. 6, pp. 2875–2884, Nov. 2021, doi: 10.1007/s42835-021-00819-0.

[3] D. Xu *et al.*, "Microstructure and electrical properties of ZrO2-doped ZnO varistor ceramics," *Journal of Materials Science: Materials in Electronics*, vol. 27, no. 1, pp. 767–771, Jan. 2016, doi: 10.1007/s10854-015-3814-5.

[4] M. H. Jali *et al.*, "Aligned vertical growth of zinc oxide nanorods on glass substrates using optimum hydrothermal synthesis technique," *Indonesian Journal of Electrical Engineering and Computer Science*, vol. 23, no. 2, pp. 694–700, Aug. 2021, doi: 10.11591/ijeecs.v23.i2.pp694-700.

[5] H. Guan *et al.*, "Fabrication and characterization of a novel varistor based on AlInGaN/GaN heterojunction epitaxy on high resistance silicon (111) substrates," *IEEE Transactions on Electron Devices*, vol. 69, no. 8, pp. 4200–4205, Aug. 2022, doi: 10.1109/TED.2022.3184645.

[6] C. Xu *et al.*, "Evaluation tests of metal oxide varistors for DC circuit breakers," *IEEE Open Access Journal of Power and Energy*, vol. 9, pp. 254–264, 2022, doi: 10.1109/OAJPE.2022.3179453.

[7] C. Zhang, Y. Hu, W. Lu, M. Cao, and D. Zhou, "Influence of TiO2/Sb2O3 ratio on ZnO varistor ceramics," *Journal of the European Ceramic Society*, vol. 22, no. 1, pp. 61–65, Jan. 2002, doi: 10.1016/S0955-2219(01)00232-1.

[8] T. T. Liu, M. H. Wang, H. P. Zhang, and Y. Z. Zhao, "Molten salt synthesis of doped nanocrystalline ZnO powders and applications in varistor ceramics," *Journal of Materials Science: Materials in Electronics*, vol. 27, no. 4, pp. 3704–3709, Apr. 2016, doi: 10.1007/s10854-015-4211-9.

[9] A. Amini, M. Rajabi, and S. M. Zahraee, "Microstructural and electrical properties of flash sintered ZnO–Bi2O3–Sb2O3 based varistors: Effect of current density with a controlled current ramp," *Materials Chemistry and Physics*, vol. 295, p. 127094, Feb. 2023, doi: 10.1016/j.matchemphys.2022.127094.

[10] C. R. Ceballos, F. Chejne, E. Pérez, A. Osorio, and A. Correa, "Study of the behavior of low voltage ZnO varistors against very fast transient overvoltages (VFTO)," *Electric Power Systems Research*, vol. 214, p. 108937, Jan. 2023, doi: 10.1016/j.epsr.2022.108937.

[11] A. Wu *et al.*, "High-performance ZnO varistor ceramics prepared by arc-induced flash sintering with low energy consumption at room temperature," *High Voltage*, vol. 7, no. 2, pp. 222–232, Apr. 2022, doi: 10.1049/hve2.12161.

[12] T. Tian *et al.*, "Novel ultrahigh-performance ZnO-based varistor ceramics," *ACS Applied Materials and Interfaces*, vol. 13, no. 30, pp. 35924–35929, Aug. 2021, doi: 10.1021/acsami.1c07735.

[13] T. E. Tsovilis and Z. Topcagic, "DC overload behavior of low-voltage varistor-based surge protective devices," *IEEE Transactions on Power Delivery*, vol. 35, no. 5, pp. 2541–2543, Oct. 2020, doi: 10.1109/TPWRD.2020.2965764.

[14] M. A. Ashraf, A. H. Bhuiyan, M. A. Hakim, and M. T. Hossain, "Microstructure and electrical properties of Ho2O3 doped Bi2O3-based ZnO varistor ceramics," *Physica B: Condensed Matter*, vol. 405, no. 17, pp. 3770–3774, Sep. 2010, doi: 10.1016/j.physb.2010.05.084.

[15] M. A. Ashraf, A. H. Bhuiyan, M. A. Hakim, and M. T. Hossain, "Microstructure and electrical properties of Sm2O3 doped Bi2O3-based ZnO varistor ceramics," *Materials Science and Engineering: B*, vol. 176, no. 11, pp. 855–860, Jun. 2011, doi: 10.1016/j.mseb.2011.04.009.

[16] A. B. Glot, R. Bulpett, A. I. Ivon, and P. M. Gallegos-Acevedo, "Electrical properties of SnO2 ceramics for low voltage varistors," *Physica B: Condensed Matter*, vol. 457, pp. 108–112, Jan. 2015, doi: 10.1016/j.physb.2014.09.026.

[17] E. Savary, S. Marinel, F. Gascoin, Y. Kinemuchi, J. Pansiot, and R. Retoux, "Peculiar effects of microwave sintering on ZnO based varistors properties," *Journal of Alloys and Compounds*, vol. 509, no. 21, pp. 6163–6169, May 2011, doi: 10.1016/j.jallcom.2011.03.048.

[18] C. W. Nahm, "Sintering effect on varistor properties and degradation behavior of ZVMB varistor ceramics," *Journal of Materials Science: Materials in Electronics*, vol. 28, no. 22, pp. 17063–17069, Nov. 2017, doi: 10.1007/s10854-017-7632-9.

[19] K. E. Merrill and G. T. Heydt, "The calculation of energy dissipation in metal oxide varistors for power distribution applications," *IEEE Transactions on Power Systems*, vol. 34, no. 5, pp. 3967–3969, Sep. 2019, doi: 10.1109/TPWRS.2019.2918957.

[20] G. H. Chen, J. Le Li, Y. Yang, C. L. Yuan, and C. R. Zhou, "Microstructure and electrical properties of Dy2O 3-doped ZnO-Bi2O3 based varistor ceramics," *Materials Research Bulletin*, vol. 50, pp. 141–147, Feb. 2014, doi: 10.1016/j.materresbull.2013.10.032.

[21] T. Tanaka, R. Tsuge, Y. Baba, Y. Tsujimoto, and N. Tsukamoto, "An approximate mathematical expression for nonlinear resistive properties of metal oxide varistor elements for FDTD simulations," *IEEE Transactions on Electromagnetic Compatibility*, vol. 62, no. 6, pp. 2638–2642, Dec. 2020, doi: 10.1109/TEMC.2020.2983200.

[22] M. K. Kerimov *et al.*, "Varistor effect in polymer-semiconductor composites," *Semiconductors*, vol. 44, no. 7, pp. 904–911, Jul. 2010, doi: 10.1134/S1063782610070134.

[23] M. S. C. Soh, M. S. Z. Abidin, S. F. A. Rahman, S. Elangkovan, and A. B. M. Rashid, "Zinc oxide-paper based sensor for photoconductive ultraviolet detection," *Indonesian Journal of Electrical Engineering and Computer Science*, vol. 20, no. 1, pp. 60–66, Oct. 2020, doi: 10.11591/ijeecs.v20.i1.pp60-66.

[24] C. W. Nahm, "Major effect on electrical properties and aging behavior of ZnO-Pr 6O 11-based varistor ceramics with small In 2O 3 doping changes," *Journal of Materials Science: Materials in Electronics*, vol. 23, no. 9, pp. 1715–1721, Sep. 2012, doi: 10.1007/s10854-012-0652-6.

[25] H. I. Hsiang, C. C. Chen, and C. C. Kao, "Effect of ZnBi2O4 and Bi2O3 addition on the densification, microstructure, and varistor properties of ZnO varistors," *Ceramics International*, vol. 49, no. 2, pp. 2244–2249, Jan. 2023, doi: 10.1016/j.ceramint.2022.09.192.

[26] M. Zhou *et al.*, "Varistor coupling method and recommendation parameters for combination wave test," *IET Science, Measurement and Technology*, vol. 17, no. 7, pp. 277–286, Sep. 2023, doi: 10.1049/smt2.12152.

[27] H. Debéda, S. Azzopardi, C. Lucat, M. P. Martin-Stempin, and P. Tardy, "Evaluation of insulated gate bipolar transistor protection with ZnO thick films varistors," *IET Power Electronics*, vol. 3, no. 1, pp. 1–10, 2010, doi: 10.1049/iet-pel.2008.0097.

BIOGRAPHIES OF AUTHORS

Faiçal Kharchouche he obtained a baccalaureate in chemistry. He holds degrees in electrical engineering from Farhat Abbas University Setif 1, Setif, in 2002 and a Ph.D. Degree in Electrical Engineering from Farhat Abbas University Setif 1, 2014. From 2006 to 2023, he was a researcher in the Dac Hr lab. Since 2009, he has been an Assistant Professor in the Department of Electrical Engineering. He has many articles and publications in the field electricity and protection of electrical appliances. He can be contacted at email: faical.kharchouche@univ-setif.dz.

Yousra Malaoui completed her Bachelor of Science degree in Electrical Engineering at the Department of Electrical Engineering at the University of Ferhat Abbas Setif. She also finished her Master of Science degree at the same department in Electrical Grid. Currently, she is a Ph.D. student at the same department and has been working on her research topic, which involves the study and elaboration of semiconductors for protection against electrical disturbances, specifically focusing on ZnO-based varistors. She can be contacted via email: yousra.malaoui@univ-setif.dz.

Omrane Bouketir is currently an associate professor at Ferhat Abbas Universiry Setif 1 since 2016. Prior to this, he has been a faculty member at several international universities namely King Fahd University of Petroleum and Minerals (KFUPM, KSA), University of Notingham Malaysia Campus (UNMC) and Multimedia University (Malaysia). Dr Omrane has more than 20 years of teaching experience in Electrical enginering area; his main research interests are in renewable energy storage systems, power electronics, and CAD systems for teretiary teaching. He can be contacted at email: omrane@univ-setif.dz.